Supplementary Information

Article

Two billion years of episodic & simultaneous websteritic and eclogitic diamond formation beneath the Orapa kimberlite cluster, Botswana

Authors

M.U. Gress[1,*], S. Timmerman[1,2], I.L. Chinn[3], J.M. Koornneef[1], E. Thomassot[4], E.A.S. van der Valk[1], K. van Zuilen[1], N. Bouden[4], G.R. Davies[1]

[1] Vrije Universiteit, De Boelelaan 1085, 1081 HV Amsterdam, The Netherlands

[2] Earth and Atmospheric Sciences, University of Alberta, Edmonton, Canada T6E 2E5

[3] De Beers Exploration, Private Bag X01, Southdale 2135, South Africa

[4] Université de Lorraine, Centre de Recherches Pétrographiques et Géochimiques (CRPG), 15 Rue Notre Dame des Pauvres, BP 20, 54 501 Vandœuvre-lès-Nancy, France

[*] Corresponding author. E-mail: m.u.gress@vu.nl

Keywords: Inclusion dating; Eclogite; Websterite; Pyroxenite; Craton; Carbon and Nitrogen isotope

Online Resource 1

1.1 Geological background

The Orapa kimberlite cluster in north-east Botswana is the site of the Orapa (OR), Damtshaa (DM), Letlhakane (LK) and (more recently) Karowe diamond mines that are 20 to 30 km apart in an area of ~ 200 km^2, in addition to ~ 60 other non-mined kimberlites. At 93.1 Ma, the kimberlites intruded into the Proterozoic Magondi Mobile Belt (Allsopp et al. 1989; Davis 1977) that is thrust over the western edge of the chemically more depleted, cooler and older Zimbabwe Craton. The thickness of the lithospheric root (250 – 300 km) increases towards the Kaapvaal Craton in the south (Fouch et al. 2004; Stiefenhofer et al. 1997). Together with the Proterozoic Limpopo Mobile Belt, these major units are part of the Kalahari Craton (Jacobs et al. 2008).

Peridotite mantle xenoliths at Letlhakane define a geotherm close to 40 mW/m^2, comparable to xenoliths from kimberlites on the Kaapvaal Craton and they show variably trace element enriched mantle signatures stabilised in the SCLM since the Archaean (Stiefenhofer et al. 1997). At Orapa, eclogite xenoliths are more prevalent, likely due to initial weathering of peridotites in the crater lake facies (Stiefenhofer et al. 1997). To date, several discrete diamond populations with distinctly different characteristics in e.g., their inclusion geochemistry and C-N isotopic record for each paragenesis have been identified in the Orapa cluster (Chinn et al. 2018; Deines and Harris 2004; Deines et al. 1993; Deines et al. 2009; Motsamai et al. 2018; Stachel et al. 2004; Timmerman et al. 2018; Timmerman et al. 2017).

Despite the generally low (< 10%) abundance of peridotitic diamonds in the Orapa cluster (Gurney et al. 1984), peridotitic diamonds at Letlhakane and Damtshaa are more abundant than at Orapa (Deines et al. 2009). In the case of Karowe, diamonds are also derived from deeper (190 – 220 km), more depleted dunitic-harzburgitic reservoirs compared to average formation depths at Orapa (160 km, 1230 ± 80°C (Motsamai et al. 2018; Stachel et al. 2004)). P- and W-type diamonds at Orapa were found to have formed at relatively shallower levels than E-types (Deines et al. 1993). At Karowe, co-genetic mineral equilibration temperatures yield diamond formation between 1260°C – 1480°C at 5 GPa (Motsamai et al. 2018). Combination of the Fe-Mg exchange thermometer (Krogh, 1988) with carbon isotopic compositions of E- and W-type diamonds suggested a ~ 25 km thick mantle zone (1125°C – 1240°C, ~ 150 – 170 km, i.e. 4.7 GPa – 5.0 GPa) beneath the entire Orapa cluster that predominantly hosts diamonds depleted in ^{13}C with $\delta^{13}C$ values < -8‰ (Deines et al. 1993; 2009).

1.2 Analytical methods

Most of the plate analyses were performed using a FT/IR Jasco-470+ instrument equipped with a Jasco Irtron IRT-30 infrared microscope. Other spectra were acquired on a Thermo-Nicolet Nexus spectrometer attached to a continuum infrared microscope. For both instruments, the same recorded spectral range (4000 to 650 cm^{-1}) and spectral resolution (4 cm^{-1}) were applied. For six plates with partly brown to yellow colouration, transects were extracted from IR maps that were compiled on a Thermo Scientific Nicolet iN10 infrared microscope at the Gemological Institute of America. The spectra were recorded in a grid with 100 µm spacing with each map consisting of 50 – 200 spectra (675 to 6000 cm^{-1}) with a resolution of 1 cm^{-1} (see Smit et al. (2018) for experimental setup). Whole-stone spectra of 246 randomly sampled gem to near-gem quality diamonds from run-of-mine ranging from 0.1 to 0.8 carat were measured using Perkin Elmer and Bruker Alpha spectrometers during the sampling campaigns at DTCB.

All spectra were processed using the automated version of DiaMap (Howell et al. 2012a; Howell et al. 2012b) to determine N content and aggregation state using absorption coefficients at 1282 cm^{-1}: [NA] = 16.5 ppm (Boyd et al. 1994) and [NB] = 79.4 ppm (Boyd et al. 1995). Selected spectra from central plates recording < 50 atomic ppm (at.ppm) N were re-processed manually using the Excel version of DiaMap, to provide greater confidence in reported values. At low nitrogen concentrations (< 200 at.ppm N) the fitting of the spectra for the aggregation state does not always work well and aggregation states flip to 0 or 100 %B. Therefore, for analyses with 0 or 100 %B and < 200 at.ppm N, the aggregation state is not reported. Given the spectral resolution and the variety of analytical setups, no distinction will be made between diamonds with very low N contents (i.e. < 20 at.ppm) and 'nitrogen-free' (Type II) spectra i.e., spectra without visible and deconvolutable nitrogen peaks.

C and N isotopes and N concentration (ESM_1.1), were measured using a large-geometry secondary ion mass spectrometer (LG-SIMS) at CRPG-Nancy, following the high-resolution procedure previously described in Gress et al. (2020). The instrument has been recently upgraded with high sensitivity Faraday cups (FC 10^{12} Ω amplifiers; Bouden et al. (2021)), which are not subject to aging (unlike electron multipliers) and are easily cross-calibrated with each other. This new type of collector offers optimal performances for secondary ion intensities varying from 1 to 2 x10^6 count per second. At these conditions, they significantly improve the statistical errors (within spot uncertainties <0.2 ‰ 2σ, Fig 3. in Bouden et al. (2021)) associated with the collection of minor masses while working in multi-collection mode at high resolution. For the purpose of diamond analyses, high-sensitive FCs significantly improve the measurement of C^{13} (mass 13) and N^{14} (as CN^- on mass 26). All analyses were achieved using a $^{133}Cs+$ primary beam (Gaussian mode), with a total acceleration voltage of 20 kV and a primary intensity of 4.2 ±0.2 nA, corresponding to a spot size of ~15 µm. Carbon-12 and -13 were detected simultaneously on FC (mass 12 on the central detector C and mass 13.003355 on H'2, using a 10^{11} Ω amplifier and a 10^{12} Ω amplifier, respectively) at a mass resolution power (MRP) of 5000 allowing the full separation of ^{13}C- and ^{12}CH-.

For N isotopes, measurements were acquired at a MRP of 9222 that guarantees the full separation of $^{26}[^{12}C^{14}N$-] and $^{26}[^{13}C^{13}C$-]. Mass 25 ($^{12}C^{13}C$- on C, using a 10^{11} Ω amplifier) and mass 26 ($^{12}C^{14}N$- on the axial position using FC2 with a 10^{12} Ω amplifier) were collected simultaneously for 5 s, followed by mass 27 ($^{14}N^{15}N$- on the axial position using an electron multiplier) after magnetic field jumping for 10 s. N-content measurements were calibrated using 6 reference materials previously characterized by Fourier Transformed Infra-Red spectroscopy at IPGP (Nam-22, -27, -56 and -114 from Cartigny et al. (2004) as well as two new diamond plates provided by D. Jacob and characterized for the present study, MC-20 and MC-24). The wide N content range of our RM collection (from 11 to 2740 at. ppm N) ensures a good calibration associated with small calibration error of ± 25 at. ppm (i.e. 5 % error for a diamond containing 500 at.ppm).

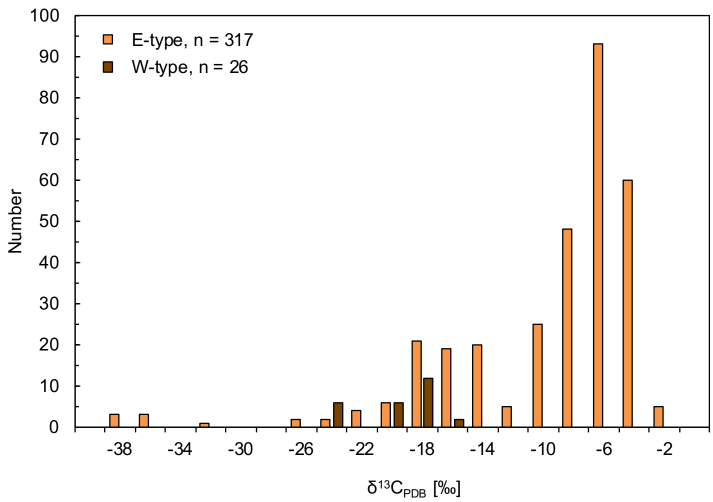

Figure ESM_1.1: $\delta^{13}C$ histogram for measurements from individual diamond growth zones on LK plates of eclogitic (E-type) and websteritic (W-type) paragenesis.

For clean lab chemistry, the inclusions were weighed and spiked with an ^{84}Sr spike, ^{87}Rb spike and a ^{149}Sm-^{150}Nd mixed spike prior to column chemistry. Chemical separation was performed in a miniaturised downstream column procedure where the Sr-columns (0.07 mL Eichrom Sr resin) were stacked on top of the TRU columns (0.23 mL Eichrom TRU resin; for details, see Koornneef et al. (2017)), followed by miniaturised endurable quartz-columns for Rb separation (0.16 mL Bio-Rad AG50x8 200-400 mesh) and miniaturised LN-resin (Eichrom 50 - 100µm; 0.74 mL) columns for Sm-Nd separation. Total procedural blanks across batches yielded ranges of 0.03 – 180.9 pg Rb, 1.67 – 89 pg Sr, 0 – 8.4 pg Sm and 0.03 – 3.65 pg Nd, respectively. All matrix fractions from column chemistry were collected and merged for trace element analyses on a Thermo X-Series II. Changes in sensitivity over time were monitored and corrected for using a BHVO-2 (~ 30,000 times diluted), which was analysed after every sample (modified after Eggins et al. (1997)). After interference correction, elemental concentrations of the matrix cuts were calculated using a two-point calibration of blank and BHVO-2 (10241 or 35478 times diluted). Subsequently, the matrix cuts were further yield-corrected using the average of 4 aliquots (with different dilution factors similar to the samples) of the ~ 1 mg BHVO-2 that was previously processed together with the samples on the columns and filtered for limits of quantification.

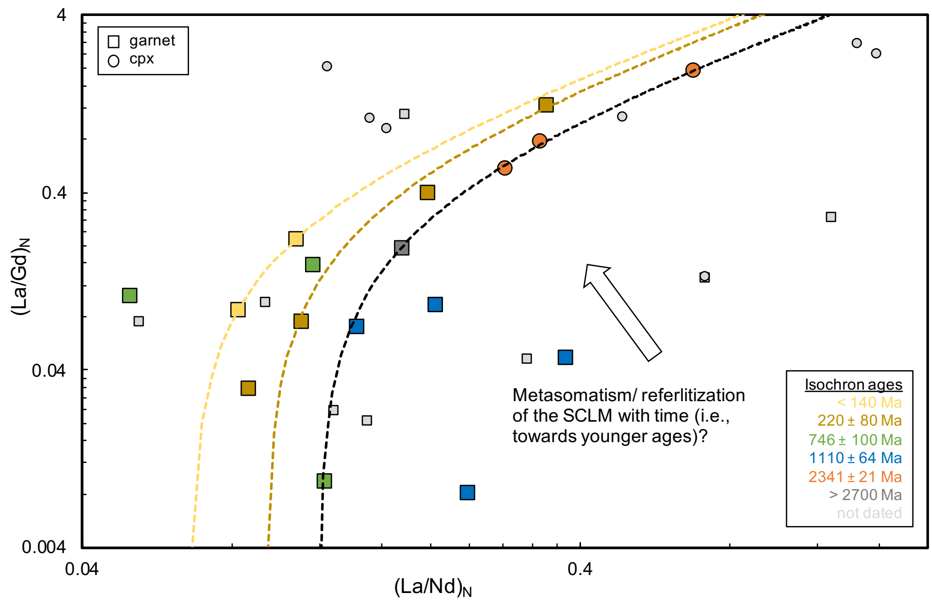

Figure ESM_1.2: Plot of $(La/Nd)_N$ versus $(La/Gd)_N$ illustrating the enrichment of LREE & Nd relative to Gd towards younger ages in eclogitic and websteritic diamonds.

Given the small amount of sample and corresponding miniature silicate matrix interacting with the column resin during chemical separation, yields for high field strength elements (HFSE) were 8 % – 24 %, 64 % – 73 % for Ba and Y and > 68 % for the REE (i.e., La and Tb to Lu), while Ce to Eu had 10 % – 40 % owing to the elution of Nd and Sm. Reported errors are fully propagated and generally range between 5 % – 30 %. Total procedural blanks were generally < 2 ppb, except for Ba (< 7.1 ppb), La (< 7.8 ppb), Zr (< 9.2 ppb) and Ti (< 900 ppb). Ratios of $(La/Nd)_N$ versus $(La/Gd)_N$ are shown to illustrate the enrichment of LREE & Nd relative to Gd (ESM_1.2).

1.3 Tectono-magmatic implications

Eclogitic – websteritic diamond formation covers almost the entire evolution of the Kalahari Craton (Fig. 7). The formation of LK224 (T_{CHUR} = 3.9 ± 1.2 Ga), *Group b*, appears to reflect initial formation of the oceanic lithosphere or craton formation around the currently accepted start of widespread modern plate tectonic processes (Condie and Kröner 2008; Shirey and Richardson 2011). The large uncertainty also does not rule out formation contemporaneous with Archaean eclogitic sulphide-bearing diamonds (3.1 – 2.9 Ga) in Botswana (Richardson et al. 2004; Shirey et al. 2008) and South Africa (Pearson and Harris 2004; Richardson et al. 2001).

The 2.34 ± 0.02 Ga age of *Group 1* diamond formation characterised by light $\delta^{13}C$ and positive $\delta^{15}N$ coincides with subduction associated with the accretion of Kenorland and the addition of the Western Terrane to the Kaapvaal Craton (Timmerman et al. 2017). Like any other reported diamond-forming event, not every diamond formation age needs to necessarily be linked to events recorded in Earth' crust. Notably, no younger (< 2.34 Ga) diamonds show such an organic-rich component in their cores and this suggests that this source was not prominent in subsequent diamond-forming events. Geodynamically, thrusting of the Magondi Belt over the Zimbabwe Craton (2.0 – 1.8 Ga) could have either acted as physical barrier or colder mantle could have prevented component C being reactivated. Only diamonds of recent age (< 220 Ma) temporally related to Karoo or kimberlite magmatism indicate mixing between component B with C.

Diamonds of *Group 2* formed at 1.70 ± 0.28 Ga and a comparable age (1.79 ± 0.1 Ga) is recorded at Jwaneng 370 km to the southwest. These latter diamonds also predominantly carry cpx inclusions

($^{87}Sr/^{86}Sr$: 0.7026 – 0.7042) and have mantle-like $\delta^{13}C$ (-8.5‰ to -6.4‰; Gress et al. (2020)). The authors related this event to the accretion of the Rehoboth Terrain between 2.0 – 1.75 Ga (Oriolo and Becker 2018; Van Schijndel et al. 2011) that also caused (re-)mobilisation of older (~ 3.0 Ga), eclogitic material in the SCLM beneath Jagersfontein, 940 km south of the Orapa cluster, and promoted the formation of eclogitic sulphide inclusion-bearing diamonds with a narrow range $\delta^{13}C$ (-9.8‰ to -3.5‰; Aulbach et al. (2009)). If true, the events would have resulted in diamond formation initiated by subduction along the entire W and NW margin of the Proto-Kalahari Craton, with restricted compositions mixing a mantle-like component (A) with subducted material (i.e., component B).

Eclogitic diamond formation at ~ 1.1 Ga (*Group 3*) has previously been inferred from composite silicates (990 ± 50 Ma; Richardson et al. (1990)) and individual sulphide inclusions (~ 1.0 Ga; Shirey et al. (2008)) from Orapa. The composite silicate age of Richardson et al. (1990), however, probably represents the median of the inclusion populations. Inclusions from three mines from the Orapa cluster record the 1100 Ma event. This E- and W-type diamond formation event appears to be regional, ~ 0.5 M km^2, extending across much of the Kalahari Craton, with pooled silicates from Premier (1150 ± 60 Ma; Richardson (1986)), and sulphide inclusions from Koffiefontein (1048 ± 120 Ma; Pearson et al. (1998)) and Jagersfontein (~ 1.1 Ga; Aulbach et al. (2009)). This age is indistinguishable from the continent-collisional event between the Kalahari Craton and Laurentia, best-dated at 1090 – 1060 Ma (Jacobs et al. 2003) and is supported by the low εNd_i (-2.6). Localised mobilisation of volatile-rich diamond-forming fluids during a collisional event would also explain the compositional heterogeneity of the inclusions because regional magmatism as suggested for Venetia P-type diamonds (Koornneef et al. 2017) would potentially overprint most of the original protolith signature and provide uniform compositions across the different locations.

Eclogitic diamond formation at 0.75 ± 0.1 Ga (*Group 4*) appears related to rifting of Rodinia that occurred along the western margin of the Kalahari between 800 – 750 Ma (Jacobs et al. 2008). A lherzolitic diamond-forming event of similar age (718 ± 49 Ma; Aulbach et al. (2018)) was reported at Victor (Superior Craton, Canada) and in an eclogitic diamond-forming event at Jwaneng (850 ± 50 Ma; Gress et al. (2020)), both apparently related to rifting in the Rodinia supercontinent. Despite this widespread rifting and supposedly favourable diamond-forming conditions with oxidizing fluids coming from the asthenosphere (Aulbach et al. 2018), so far, this age is rare among diamonds from Superior and Kalahari Cratons but may have been overlooked owing to the averaging effect of composite inclusion dating techniques. Such asthenospheric fluids may have provided the heat necessary to initiate the redistribution of carbon in the SCLM and mixing with the asthenosphere-derived carbon.

Inclusions formed in the younger growth events (< 745 Ma) are derived from fluids with increasingly fractionated LREE (higher LREE/MREE ratios) possibly suggesting greater scavenging of LREE from the SCLM (Figure ESM_1.2). Diamond formation at 220 Ma (*Group 5*) was potentially related to the amalgamation and breakup of Pangea (320 - 185 Ma; Veevers (2004)). The LREE enriched nature of the garnets together with the mantle-like C-N compositions in the majority of diamonds supports the involvement of a regional magmatic event such as the Karoo-Ferrar LIP (183 ± 0.5 Ma; Svensen et al. (2012)).

The youngest diamonds (*Group c*) in the Orapa cluster are clearly related to kimberlite magmatism in the region (< 140 Ma). The marked trace element enrichment of the metasomatic fluids that formed the inclusions (Fig. 5) resembles that of extreme kimberlitic magmas such as orangeites that were active in the region from 143 to 117 Ma (Jelsma et al. 2009). Eclogitic diamond formation close to the kimberlite eruption age has been previously implied for diamonds from Premier and Koffiefontein (Pearson et al. 1998; Richardson 1986) or Jwaneng (Timmerman et al. 2019). Such young Phanerozoic ages are also common for fibrous diamonds (Gurney et al. 2010) but clear genetic relationships with monocrystalline diamonds (Jablon and Navon 2016; Rege et al. 2010) were only established recently (Krebs et al. 2019). The SCLM beneath the Kaapvaal Craton records widespread evidence of metasomatism related to, or immediately prior to, kimberlite eruption (Grégoire et al. 2003; 2007; Simon et al. 2003). Coupled with the marked variation in the εNd_i (-42.5 to -2.2) and $\delta^{13}C$ (-21.3‰ to -4.9‰) of the youngest diamonds, this suggests that fluid-rock interaction during diamond formation involved low-volume fluids such that the heterogeneity of eclogitic and websteritic protoliths in the SCLM is reflected in diamond compositions.

References

Allsopp H, Bristow J, Smith C, Brown R, Gleadow A, Kramers J, Garvie O (1989) A summary of radiometric dating methods applicable to kimberlites and related rocks Kimberlites and related rocks 1:343-357

Aulbach S, Creaser RA, Stachel T, Heaman LM, Chinn IL, Kong J (2018) Diamond ages from Victor (Superior Craton): Intra-mantle cycling of volatiles (C, N, S) during supercontinent reorganisation Earth Planet Sc Lett 490:77-87

Aulbach S, Shirey SB, Stachel T, Creighton S, Muehlenbachs K, Harris JW (2009) Diamond formation episodes at the southern margin of the Kaapvaal Craton: Re–Os systematics of sulfide inclusions from the Jagersfontein Mine Contrib Mineral Petr 157:525-540

Bouden N et al. (2021) Triple Oxygen Isotope Measurements by Multi-Collector Secondary Ion Mass Spectrometry. Front Earth Sci 8:601169

Boyd S, Kiflawi I, Woods G (1994) The relationship between infrared absorption and the A defect concentration in diamond Philos Mag B 69:1149-1153

Boyd S, Kiflawi I, Woods G (1995) Infrared absorption by the B nitrogen aggregate in diamond Philos Mag B 72:351-361

Cartigny P, Stachel T, Harris JW, Javoy M (2004) Constraining diamond metasomatic growth using C- and N-stable isotopes: examples from Namibia Lithos 77:359-373

Chinn IL, Perritt SH, Stiefenhofer J, Stern RA (2018) Diamonds from Orapa Mine show a clear subduction signature in SIMS stable isotope data Mineralogy and Petrology 112:197-207

Condie KC, Kröner A (2008) When did plate tectonics begin? Evidence from the geologic record. In: When did plate tectonics begin on planet Earth, vol 440. Geological Society of America Special Papers, pp 281-294

Davis GL The ages and uranium contents of zircons from kimberlites and associated rocks. In: International Kimberlite Conference: Extended Abstracts, 1977. pp 67-69

Deines P, Harris JW (2004) New insights into the occurrence of 13 C-depleted carbon in the mantle from two closely associated kimberlites: Letlhakane and Orapa, Botswana Lithos 77:125-142

Deines P, Harris JW, Gurney JJ (1993) Depth-related carbon isotope and nitrogen concentration variability in the mantle below the Orapa kimberlite, Botswana, Africa Geochim Cosmochim Ac 57:2781-2796

Deines P, Stachel T, Harris JW (2009) Systematic regional variations in diamond carbon isotopic composition and inclusion chemistry beneath the Orapa kimberlite cluster, in Botswana Lithos 112:776-784

Eggins S et al. (1997) A simple method for the precise determination of≥ 40 trace elements in geological samples by ICPMS using enriched isotope internal standardisation Chemical geology 134:311-326

Fouch MJ, James DE, VanDecar JC, Van der Lee S, Group KS (2004) Mantle seismic structure beneath the Kaapvaal and Zimbabwe Cratons South African Journal of Geology 107:33-44

Grégoire M, Bell DR, Le Roex AP (2003) Garnet Lherzolites from the Kaapvaal Craton (South Africa): Trace Element Evidence for a Metasomatic History Journal of Petrology 44:629-657

Gress MU, Koornneef JM, Thomassot E, Chinn IL, van Zuilen K, Davies GR (2020) Sm-Nd isochron ages coupled with CN isotope data of eclogitic diamonds from Jwaneng, Botswana Geochim Cosmochim Ac 293:1-17

Gurney J, Harris JW, Rickard RS (1984) Silicate and oxide inclusions in diamonds from the Orapa Mine, Botswana Kimberlites II: the mantle and crust–mantle relationships Elsevier, Amsterdam:3-9

Gurney J, Helmstaedt H, Richardson S, Shirey S (2010) Diamonds through time Economic Geology 105:689-712

Howell D, O'Neill C, Grant K, Griffin W, Pearson N, O'Reilly S (2012a) μ-FTIR mapping: distribution of impurities in different types of diamond growth Diam Relat Mater 29:29-36

Howell D et al. (2012b) Platelet development in cuboid diamonds: insights from micro-FTIR mapping Contrib Mineral Petr 164:1011-1025

Jablon BM, Navon O (2016) Most diamonds were created equal Earth Planet Sc Lett 443:41-47

Jacobs J, Bauer W, Fanning C (2003) New age constraints for Grenville-age metamorphism in western central Dronning Maud Land (East Antarctica), and implications for the palaeogeography of Kalahari in Rodinia International Journal of Earth Sciences 92:301-315

Jacobs J, Pisarevsky S, Thomas RJ, Becker T (2008) The Kalahari Craton during the assembly and dispersal of Rodinia Precambrian Research 160:142-158

Jelsma H, Barnett W, Richards S, Lister G (2009) Tectonic setting of kimberlites Lithos 112:155-165

Koornneef JM, Gress MU, Chinn IL, Jelsma HA, Harris JW, Davies GR (2017) Archaean and Proterozoic diamond growth from contrasting styles of large-scale magmatism Nat Commun 8:648 doi:10.1038/s41467-017-00564-x

Krebs M, Pearson D, Stachel T, Laiginhas F, Woodland S, Chinn I, Kong J (2019) A common parentage-low abundance trace element data of gem diamonds reveals similar fluids to fibrous diamonds Lithos 324:356-370

Motsamai T, Harris JW, Stachel T, Pearson DG, Armstrong J (2018) Mineral inclusions in diamonds from Karowe Mine, Botswana: super-deep sources for super-sized diamonds? Mineralogy and Petrology 112:169-180

Oriolo S, Becker T (2018) The Kalahari Craton, Southern Africa: from Archean crustal evolution to Gondwana amalgamation. In: Geology of Southwest Gondwana. Springer, pp 133-159

Pearson DG, Harris JW (2004) Age constraints for diamonds from Koffiefontein mine, S. Africa, a Re-Os isotope and N-aggregation study Age 5:21

Pearson DG, Shirey S, Harris J, Carlson R (1998) Sulphide inclusions in diamonds from the Koffiefontein kimberlite, S Africa: constraints on diamond ages and mantle Re–Os systematics Earth Planet Sc Lett 160:311-326

Rege S, Griffin WL, Pearson N, Araújo D, Zedgenizov D, O'Reilly SY (2010) Trace-element patterns of fibrous and monocrystalline diamonds: insights into mantle fluids Lithos 118:313-337

Richardson SH (1986) Latter-day origin of diamonds of eclogitic paragenesis Nature 322:623-626

Richardson SH, Erlank AJ, Harris JW, Hart SR (1990) Eclogitic diamonds of Proterozoic age from Cretaceous kimberlites Nature 346:54-56

Richardson SH, Shirey S, Harris J, Carlson R (2001) Archean subduction recorded by Re–Os isotopes in eclogitic sulfide inclusions in Kimberley diamonds Earth Planet Sc Lett 191:257-266

Richardson SH, Shirey SB, Harris JW (2004) Episodic diamond genesis at Jwaneng, Botswana, and implications for Kaapvaal craton evolution Lithos 77:143-154

Shirey SB, Richardson SH (2011) Start of the Wilson Cycle at 3 Ga Shown by Diamonds from Subcontinental Mantle Science 333:434-436 doi:10.1126/science.1206275

Shirey SB, Richardson SH, Harris JW Mesoarchean to Mesoproterozoic Re-Os ages for sulfide inclusions in Orapa diamonds and implications for Kaapvaal-Zimbabwe craton development. In: International Kimberlite Conference: Extended Abstracts, 2008.

Simon NSC, Carlson RW, Pearson DG, Davies GR (2007) The origin and evolution of the Kaapvaal cratonic lithospheric mantle Journal of Petrology 48:589-625

Simon NSC, Irvine GJ, Davies GR, Pearson DG, Carlson RW (2003) The origin of garnet and clinopyroxene in “depleted” Kaapvaal peridotites Lithos 71:289-322

Smit KV, D’Haenens-Johansson UF, Howell D, Loudin LC, Wang W (2018) Deformation-related spectroscopic features in natural Type Ib-IaA diamonds from Zimmi (West African craton) Mineralogy and Petrology 112:243-257

Stachel T, Viljoen K, McDade P, Harris J (2004) Diamondiferous lithospheric roots along the western margin of the Kalahari Craton—the peridotitic inclusion suite in diamonds from Orapa and Jwaneng Contrib Mineral Petr 147:32-47

Stiefenhofer J, Viljoen K, Marsh J (1997) Petrology and geochemistry of peridotite xenoliths from the Letlhakane kimberlites, Botswana Contrib Mineral Petr 127:147-158

Svensen H, Corfu F, Polteau S, Hammer Ø, Planke S (2012) Rapid magma emplacement in the Karoo Large Igneous Province Earth Planet Sc Lett 325-326:1-9

Timmerman S, Chinn IL, Fisher D, Davies GR (2018) Formation of unusual yellow Orapa diamonds Mineralogy and Petrology 112:209-218

Timmerman S, Koornneef JM, Chinn IL, Davies GR (2017) Dated eclogitic diamond growth zones reveal variable recycling of crustal carbon through time Earth Planet Sc Lett 463:178-188

Timmerman S et al. (2019) U-Th/He systematics of fluid-rich ‘fibrous’ diamonds–Evidence for pre-and syn-kimberlite eruption ages Chemical Geology 515:22-36

Van Schijndel V, Cornell DH, Hoffmann K-H, Frei D (2011) Three episodes of crustal development in the Rehoboth Province, Namibia Geological Society, London, Special Publications 357:27-47

Veevers J (2004) Gondwanaland from 650–500 Ma assembly through 320 Ma merger in Pangea to 185–100 Ma breakup: supercontinental tectonics via stratigraphy and radiometric dating Earth-Science Reviews 68:1-132